

---

# REPARO: Compositional 3D Assets Generation with Differentiable 3D Layout Alignment

---

Haonan Han<sup>1\*</sup> Rui Yang<sup>2\*</sup> Huan Liao<sup>1\*</sup> Jiankai Xing<sup>1</sup> Zunnan Xu<sup>1</sup>

Xiaoming Yu<sup>3</sup> Junwei Zha<sup>3</sup> Xiu Li<sup>1†</sup> Wanhua Li<sup>4†</sup>

<sup>1</sup>Tsinghua University <sup>2</sup>The University of Hong Kong

<sup>3</sup>Tencent Meeting <sup>4</sup>Harvard University

hhn22@mails.tsinghua.edu.cn rayyang0116@gmail.com

## Abstract

Traditional image-to-3D models often struggle with scenes containing multiple objects due to biases and occlusion complexities. To address this challenge, we present REPARO, a novel approach for compositional 3D asset generation from single images. REPARO employs a two-step process: first, it extracts individual objects from the scene and reconstructs their 3D meshes using off-the-shelf image-to-3D models; then, it optimizes the layout of these meshes through differentiable rendering techniques, ensuring coherent scene composition. By integrating optimal transport-based long-range appearance loss term and high-level semantic loss term in the differentiable rendering, REPARO can effectively recover the layout of 3D assets. The proposed method can significantly enhance object independence, detail accuracy, and overall scene coherence. Extensive evaluation of multi-object scenes demonstrates that our REPARO offers a comprehensive approach to address the complexities of multi-object 3D scene generation from single images. The demo page have been available at <https://reparo2024.github.io/>.

## 1 Introduction

The swift advancement of the 2D diffusion models and technologies, like neural rendering [34] and Score Distillation Sampling (SDS) [39], have greatly enhanced the efficient generation of high-quality 3D assets. This progress empowers creators in augmented reality (AR) / virtual reality (VR), gaming, filmmaking, and more [47, 24, 20]. Advanced simulation systems used in real-world engineering and entertainment scenarios often require settings that involve the combination of multiple objects. However, traditional text-to-3D [39, 25, 58] and image-to-3D [33, 49, 30, 27] generation methods, while effective in creating single-object scenes, face significant challenges in reconstruct complex multi-object scenes accurately from limited references. This is because most 3D samples feature a single centrally located object in the dataset, and image-to-3D models typically recenter the object during preprocessing, resulting in an inherent center bias in these models. Thus, they often struggle with the textures and details of occluded objects, which can be mistakenly perceived as a single entity, leading to issues that separate but occluded assets "sticking" together, as shown in Figure 2 (d).

This challenge prompted us to consider: *how to build a 3D generation pipeline that can independently manage multi-object assets?* To overcome the above limitations, our approach involves decomposing the scene into individual assets initially and then reassembling and globally optimizing their layout. Such a two-step process significantly enhances the fidelity and independence of each object within

---

\*Equal contribution

†Corresponding author

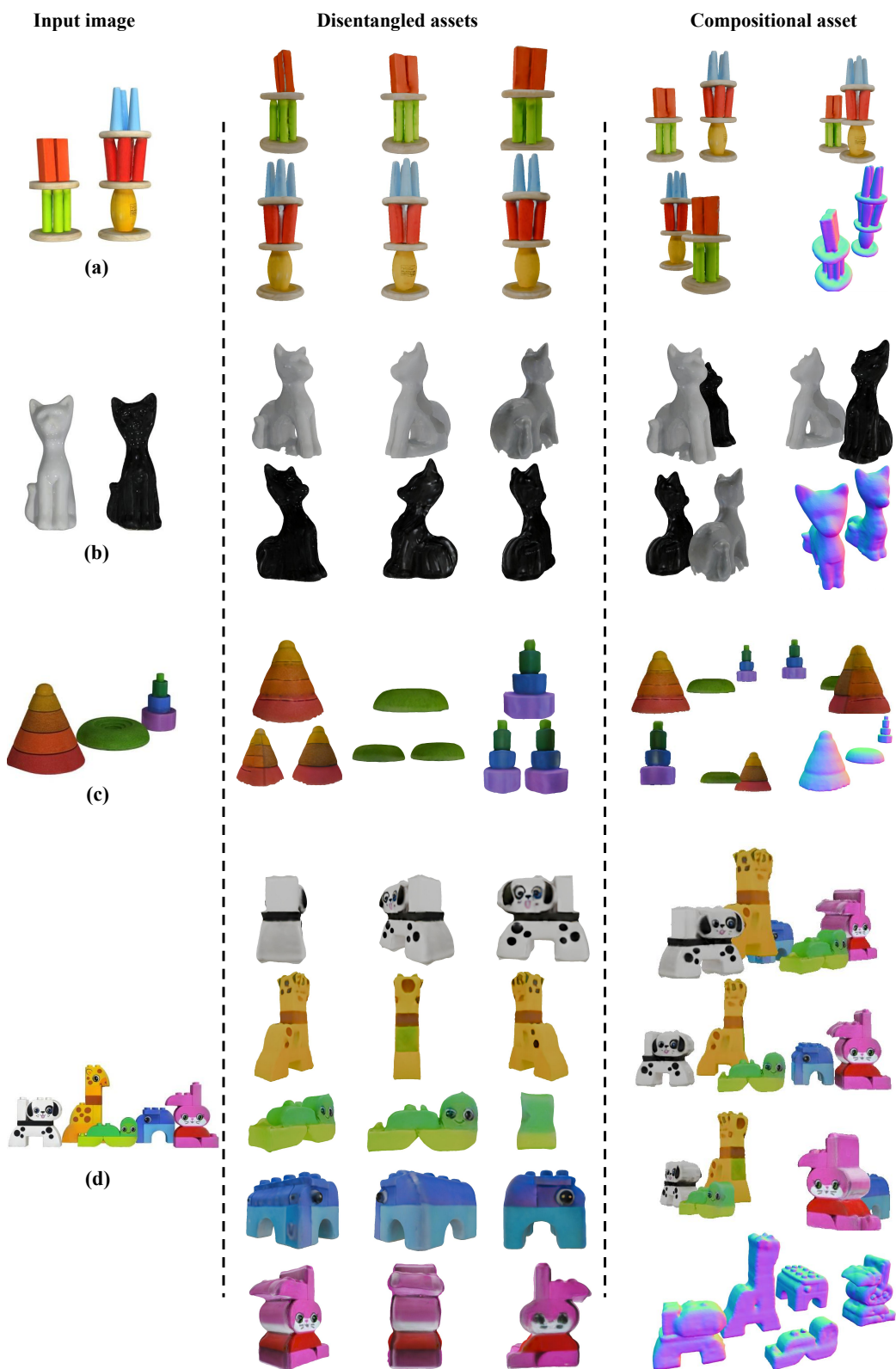


Figure 1: Compositional 3D assets generated by our REPARO.

the overall scene, addressing the inherent difficulties in handling complex occlusions and interactions among multiple objects.

Another key difficulty of multi-object compositional 3D generation is understanding and implementing context and relational dynamics between objects within a scene. This limitation stems not only from the intricacy of the geometric representation of 3D content [34, 16, 52] but also the fact that existing 3D datasets focus predominantly on a single object with very limited examples of multiple interacting objects. Recently, some studies have begun to explore the multi-object compositional 3D generation. Recent work [12] synthesizes compositional 3D scenes from either scene graphs or unstructured text descriptions. However, given the limited information conveyed by text descriptions, we take single-image as guidance and integrate differentiable 3D layout alignment.

During the assembly and layout alignment phase, our method integrates each object into a unified coordinate system. We employ differentiable rendering techniques to refine the spatial arrangement of each object. Notably, instead of using the typical pixel-wise  $L_2$  loss common in differentiable rendering, we utilize the Optimal Transport (OT) algorithm to facilitate a global one-to-one pixel matching between the rendered image and the reference image. Moreover, we propose incorporating high-level semantic features into the loss function of differentiable rendering, enhancing the model’s ability to maintain context and coherence among the objects.

Additionally, the ability to create interactive environments where users can manipulate individual elements without disrupting the overall scene’s structure and realism is also vital. Traditional 3D generation models often produce assets tied to a single mesh, complicating the task for game designers and graphic artists who need to segment these meshes using specialized tools—a process that does not ensure the quality of the segmented assets. Our targeted approach facilitates the individual generation of each asset, which can then be assembled as per the original design. This method eliminates the need for complex segmentation and joining operations, as our meshes are generated at the instance level within the scene, thus simplifying the workflow and enhancing usability for end-users.

To summarize, our methodology **REPARO** comprises two distinct phases: individual object reconstruction and combined scene optimization. Initially, we isolate each target object from the provided image and complete any occluded sections, then reconstruct their 3D meshes employing off-and-shelf 3D generation models. Subsequently, we refine the spatial configuration of these meshes through differentiable rendering, aiming to achieve a coherent layout of the scene. REPARO enhances object independence and detail accuracy, especially in occluded sections. Meanwhile, REPARO maintains not only the visual-spatial arrangement but also contextual consistency across the reconstructed scene.

To assess our approach, we selected 20 scenes from the GSO dataset [7], each containing multiple objects (ranging from 2 to 6 sub-objects) for quantitative testing. Additionally, we gathered 20 more images featuring multiple objects for qualitative analysis. This comprehensive evaluation demonstrates that our method, REPARO, offers significant improvements over previous techniques in ensuring the quality of assets, managing multiple assets, and processing occlusion.

Our contributions are summarized as follows:

1. We introduce **REPARO**, a novel approach that decomposes complex scenes into individual 3D components and then reconstructs them into accurate, high-quality multi-object scenes, enhancing object independence and detail.
2. We propose a long-range appearance loss term for the differentiable rendering to optimize the layout of 3D assets. This loss term uses the optimal transport algorithm to find a pixel match between the rendered image and the reference image, thus obtaining long-range correspondences. Then, we utilize RGB color, depth value, and position distance at the same time.
3. We propose a high-level semantic loss term for the layout alignment, significantly improving the contextual coherence and interactive potential of generated 3D scenes.

## 2 Related Work

**Text-to-3D generation.** Early exploration in 3D generation based on text [62, 34, 35, 55, 36, 41, 15] relied on a large-scale pre-trained model of text and image, CLIP [41], to optimize representation as the prior. In light of the promising capability of diffusion models, some works [39, 25, 1, 58, 42, 21,

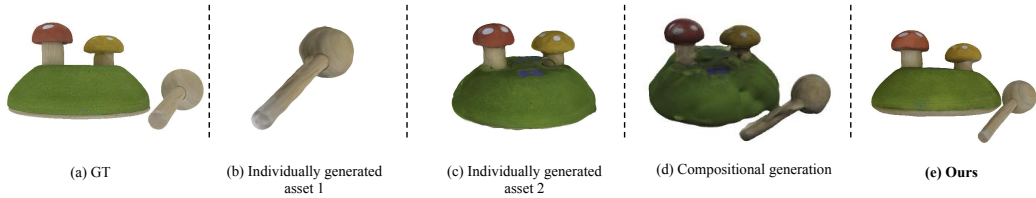


Figure 2: Qualitative comparison of generated 3D assets of the single object and multiple objects. (b) and (c) are generated 3D assets of the single object assets using DreamGaussian [48]; (d) is a 3D asset of multiple objects generated by DreamGaussian [48]; and (e) is our result.

[56, 43] introduce Score Distillation Sampling (SDS) to narrow the gap between novel view images rendered from 3D representation and diffusion prior. Recent works [48, 65, 3, 23] have used 3D Gaussian Splatting [16] instead of NeRF [34] for 3D generation, due to the fact that this efficient 3D representation shows excellent quality in reconstruction tasks.

**Image-to-3D generation.** Differing from the ambiguity and diversity associated with textual description, 3D generation based on a single image predominantly concentrates on maintaining geometric and textural consistency between the generated assets and the input images. Some early works [33, 49] used 2D diffusion models as prior knowledge to guide the training of 3D representation of the object in input images. However, with the enrichment of 3D data [6, 5], a series of adapting fine-tuned diffusion models [29, 44, 28, 40, 27, 60, 67] represented by Zero-1-to-3 [30] have been continuously developed. Subsequently, further advancements [31, 45, 46, 32] have been proposed, which offer improved quality and multi-view consistency. More recently, a new paradigm [14, 63] getting rid of diffusion models relying on camera view as condition has emerged, mainly based on transformer architecture [53] and triplane [34] representation.

### Compositional 3D generation.

In contrast to single-object reconstruction, generating complex 3D assets that contain multiple objects requires meticulous attention to detail not only for individual objects but also for their spatial relationships and occlusions. Responding to the challenges in achieving realistic and coherent compositions, related studies are mostly split into two sub-tasks constructing local single objects and modeling global scenes.

To configure the layout of the scene and place objects, the 3D geometric surface model [11] is constructed through compositing the retrieved and interactive segmented 3D meshes. Part-aware generative model [50] is proposed for editable 3D shape synthesis. Bounding boxes [38] and text prompts [57] are utilized for scene component creation. Explicit Gaussian radiance field [54] is used as guidance of object compositions. Scene graphs [12] are used to generate compositional 3D scenes by exploiting node and edge information. Large language models (LLMs) are integrated into pipeline [26] as a 3D layout interpreter. Method [2] applied spatially-aware score distillation sampling to guide the positions of 3D assets, while work [9] learned 3D NeRF layouts for text-prompted scenes. Recent work [64] employed a 2D semantic layout map as an input condition to generate compositional 3D scenes. Meanwhile model [66] leverages Gaussian Splatting and LLMs to create complex 3D scenes from textual descriptions. Differently, our method focuses on directly generating multiple high-quality 3D assets from a single image containing complex compositional objects, while the positions of assets are aligned with the layout of the input image.

## 3 Method

The field of 3D generation is advancing rapidly, with numerous image-to-3D models [48, 51] now capable of generating 3D assets from a single image. However, these models typically focus on individual objects, making it challenging to apply them to scenes containing multiple objects. To address this limitation, we propose **REPARO** for compositional 3D object generation from a single image. Our approach consists of two steps: (1) Extracting each target object from the given image and reconstructing their 3D meshes using off-the-shelf 3D reconstruction models. (2) Optimizing the parameters of each mesh through differentiable rendering so as to align their layout. In the following section, we provide a detailed explanation of these two steps.

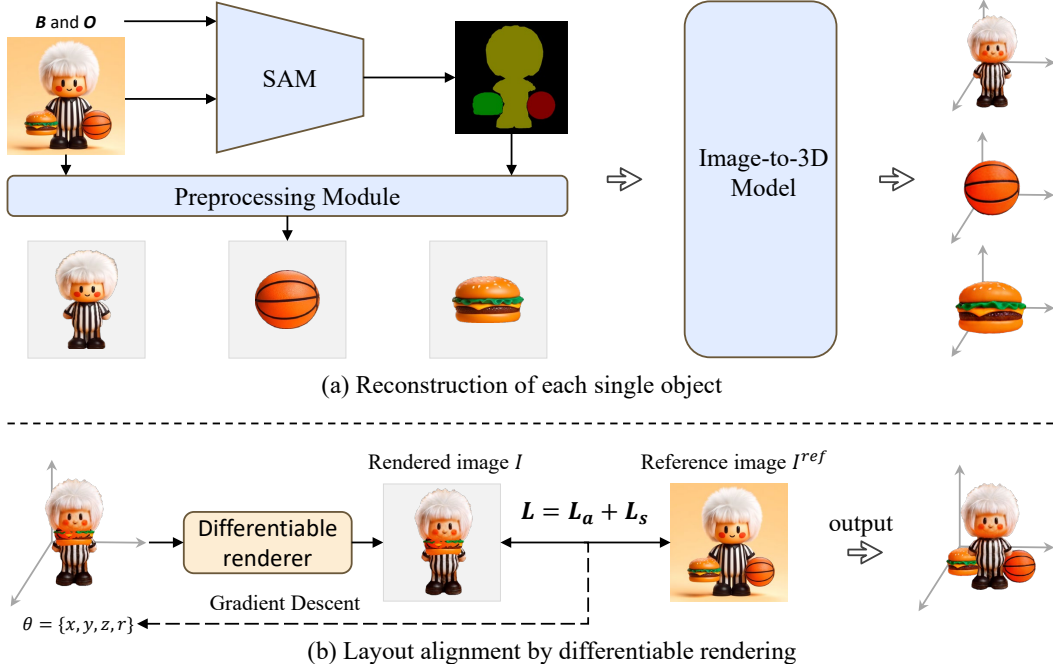


Figure 3: The diagram of the proposed REPARO. (a) is the pipeline to reconstruct the 3D asset of each object in the reference image.  $B$  and  $O$  denote bounding boxes and occlusion information of each object, respectively. If an object is occluded, the preprocessing module will complement it using the inpainting model. (b) is the process of layout alignment based on differentiable rendering. The parameters of reconstructed meshes are optimized by gradient descent. The loss function  $L$  (Eq. 9) consists of the long-range appearance loss  $L_a$  and the high-level semantic loss  $L_s$ .

### 3.1 Reconstruction of Each Single Object

Since most data samples in 3D datasets only have one object located centrally within the image, and most image-to-3D models recenter the object in the preprocessing step, there is an inherent center bias in these models. As a result, the generated 3D assets for single objects are better than for multiple objects. As shown in Figure 2, DreamGaussian [48] can generate the sound 3D asset for a single object, but it fails in generation for multiple objects. Instead of reconstructing 3D assets of multiple objects at the same time, our **REPARO** first focuses on extracting individual objects from images containing several objects and then generating their 3D assets using image-to-3D models.

**Object Extraction.** As illustrated in Figure 3 (a), given an image  $I^{ref}$  with the bounding boxes  $B$  and occlusion information  $O$ , we use the foundation model SAM [18] to segment each object and obtain their binary masks  $M$ . For occluded objects, we utilize a Stable-Diffusion-based inpainting model to reconstruct the occluded parts in the preprocessing module, thereby obtaining complete RGB priors for each object. Plus, we resize and crop the images to centralize the involved objects, which adapts to the center bias of existing image-to-3D models.

**Single Object Reconstruction.** After that, we employ off-the-shelf image-to-3D models, such as Dreamgaussian [48], to generate the corresponding 3D assets for each obtained object.

### 3.2 Layout Alignment by Differentiable Rendering

After obtaining every single object, we need a layout. To achieve the goal, first, we put every object together in one coordinate system as demonstrated in Figure 3 (b), then we use differentiable rendering techniques [19, 22, 61] to optimize the layout of each object. Differentiable rendering aims to recover the scene parameters  $\theta$  from reference image(s)  $I^{ref}$  through analysis by synthesis process. Given an initial estimation of the scene, differentiable rendering can produce a rendered image  $I$  together with the gradients with respect to arbitrary scene parameters  $\theta$ . Briefly, the gradient can be

represented as:

$$\frac{\partial I}{\partial \theta} = \left[ \frac{\partial I(p_1)}{\partial \theta}, \dots, \frac{\partial I(p_N)}{\partial \theta} \right] = \left[ \frac{\partial I_1}{\partial \theta}, \dots, \frac{\partial I_N}{\partial \theta} \right], \quad (1)$$

where  $p_i$  refers to the position of  $i$ -th pixel,  $I(p_i)$  is the RGB color of  $i$ -th pixel, and  $N$  is the total number of pixels. We denote  $I(p_i) = I_i$  for simplicity in the following. Combining with the loss function between rendered and reference image, we can leverage a gradient-descent-based method like Adam [17] to optimize the scene parameters of interest, like geometry, material, or lights. According to the chain rule, the derivative of the loss function  $L(I, I^{ref})$  with respect to scene parameters  $\theta$  is:

$$\frac{\partial L}{\partial \theta} = \frac{\partial L}{\partial I} \cdot \frac{\partial I}{\partial \theta}. \quad (2)$$

Specifically, for our task, since we have put every generated object in the same coordinate system, the layout of objects in the initial rendered image and reference image may have quite large differences. Such a case is not suitable for the commonly used pixel-wised  $L_2$  loss function and differentiable rendering methods that only compute color derivatives. Imagine that when an object in the reference image has no overlapped area with it in the rendered image, the  $L_2$  loss will not change when we slightly move the object, the gradients of the loss function could get stuck in an undesired local minima and not indicate the right way for optimization. To mitigate this issue, we propose to introduce a loss function that could find the global correspondences. For one thing, inspired by previous work [13, 61], we use the optimal transport algorithm to find a match between the rendered image and the reference image, thus obtaining long-range correspondences. For another thing, we utilize the feature embedding from the visual backbone to get semantic correspondences.

### 3.2.1 Long-range Appearance Loss Term

Optimal transport theory describes the following problem: suppose there are  $N$  suppliers and  $M$  demanders within a region. The  $i$ -th supplier holds  $s_i$  units of goods, and the  $j$ -th demander needs  $d_j$  units of goods. The transportation cost per unit of goods from  $i$ -th supplier to  $j$ -th demander is  $c_{ij}$ . The goal of the optimal transport algorithm is to find a transportation matrix  $T = \{T_{ij} \mid i = 1, \dots, N; j = 1, \dots, M\}$  that minimizes the total transportation cost:

$$\min_T \sum_{i=1}^N \sum_{j=1}^M T_{ij} c_{ij}, \quad s.t. \quad \sum_{i=1}^N T_{ij} = d_j, \quad \sum_{j=1}^M T_{ij} = s_i, \quad \sum_{i=1}^N s_i = \sum_{j=1}^M d_j, \quad T_{ij} > 0. \quad (3)$$

In our layout alignment, we consider all the pixels in the rendered image  $I$  as suppliers and all the pixels in the reference image  $I^{ref}$  as demanders, where  $N = M$  and  $s_i = d_j = 1$ . For the cost, instead of only considering RGB color distance between  $i$ -th pixel and  $j$ -th pixel, we define it based on RGB color, depth value, and position distance at the same time:

$$c_{ij} = \alpha \cdot \|I_i - I_j^{ref}\|_2 + \beta \cdot \|D_i - D_j^{ref}\|_2 + \gamma \cdot \|p_i - p_j\|_2, \quad (4)$$

where  $p_i$  and  $p_j$  refer to the screen space position of  $i$ -th pixel and  $j$ -th pixel, respectively;  $D$  is the depth map predicted from the rendered image  $I$  using a frozen depth foundation model  $F_D(\cdot)$ ;  $D_i$  denotes the depth value of  $i$ -th pixel; and  $\alpha$ ,  $\beta$ , and  $\gamma$  are hyper-parameters.

Based on Eq. 3 and Eq. 4, we can obtain a transport matrix  $T$  using Sinkhorn divergences [4].  $T$  recording a one-to-one mapping between the rendered image  $I$  and the reference image  $I^{ref}$ . In other words, we can find a target pixel for each pixel in the rendered image. Formally, we define  $I_{\sigma(i)}^{ref}$  is the target pixel of  $I_i$ , where  $\sigma(\cdot)$  is the one-to-one mapping function from the transport matrix  $T$ . In addition, rather than taking only RGB color distance as the differentiable rendering loss, we also consider RGB color, depth value, and position distance together as Eq. 4. Accordingly, our appearance loss function can be expressed as:

$$L_\alpha(I, I^{ref}) = \frac{1}{N} \sum_i^N \left( \alpha \cdot \|I_i - I_{\sigma(i)}^{ref}\|_2 + \beta \cdot \|D_i - D_{\sigma(i)}^{ref}\|_2 + \gamma \cdot \|p_i - p_{\sigma(i)}\|_2 \right). \quad (5)$$

Here,  $N$  denotes the number of pixels of the rendered image, and the settings of all hyper-parameters are consistent with Eq. 4. To propagate the gradient of the pixel position to the scene parameter,

we can define the pixel position as the projection of the shading point used for this pixel in the rasterization process as DROT [61]. According to Eq. 2 and the chain rule, the derivative of  $L_a$  with respect to scene parameters  $\theta$  is:

$$\frac{\partial L_a}{\partial \theta} = \frac{\partial L_a}{\partial I} \cdot \frac{\partial I}{\partial \theta} + \frac{\partial L_a}{\partial D} \cdot \frac{\partial F_D}{\partial I} \cdot \frac{\partial I}{\partial \theta} + \frac{\partial L_a}{\partial p} \cdot \frac{\partial p}{\partial \theta} \quad (6)$$

Note that since we freeze the depth model  $F_D(\cdot)$ , the gradients will totally contribute to scene parameters. As the mapping function  $\sigma(\cdot)$  considers the long-range correspondence, our appearance loss term can also leverage long-range information during differentiable rendering.

### 3.2.2 High-level Semantic Loss Term

To enhance the semantic information during the alignment process, we further propose incorporating high-level features into the loss function of differentiable rendering. Our semantic loss term is defined as:

$$L_s(I, I^{ref}) = \frac{1}{K} \sum_i^K \|f_i - f_i^{ref}\|_2, \quad (7)$$

where  $f_i$  and  $f_i^{ref}$  are the  $i$ -th embedding in the feature map  $f$  and  $f^{ref}$ , respectively;  $f$  and  $f^{ref}$  are extracted using a frozen DINO-v2 [37] backbone  $F(\cdot)$ ; and  $K$  is the total number of embedding from the last hidden state. Based on this term, we can align the semantic relation between the rendered image and reference image from part to part. According to Eq. 2, the derivative of  $L_s$  with respect to layout parameters  $\theta$  is:

$$\frac{\partial L_s}{\partial \theta} = \frac{\partial L_s}{\partial F} \cdot \frac{\partial F}{\partial I} \cdot \frac{\partial I}{\partial \theta} \quad (8)$$

So far, we have integrated the proposed loss terms together to align the layout of multiple reconstructed 3D objects:

$$L(I, I^{ref}) = \lambda L_a(I, I^{ref}) + (1 - \lambda) L_s(I, I^{ref}), \quad (9)$$

where  $\lambda$  is a hyper-parameter to adjust the weight between appearance and semantic loss term. In practice, we align the layout by optimizing the object’s translation parameter  $t = \{x, y, z\}$  and rotation parameter  $r$ . Thanks to the proposed loss function, we can get the layout of the compositional 3D assets through differentiable rendering.

## 4 Experiments

### 4.1 Implementation details

In the reconstruction of 3D assets from a single object, we utilize SAM-ViT-H [18] as the segmentation model to obtain masks corresponding to each bounding box. In the preprocessing module, we extract images of the objects using these masks and subsequently resize and crop the images to center the objects. We then apply the Stable Diffusion-based inpainting model<sup>3</sup> to address occlusions in the objects. During the generation of 3D assets from a single object, we employ the DreamGaussian [48] and TripoSR [51]. For layout alignment, we use Nvdiffrast [19] as our differentiable rendering framework. During the differentiable rendering process, we optimize the translation  $x, y, z$ , and rotation  $r$  parameters of each 3D asset using gradient descent. Specifically, we employ the Adam optimizer [17] with a learning rate of 0.02 and a weight decay of 0.999. The total number of iterations is set to 500. Throughout the experiment, both the reference and rendered images are maintained at a resolution of  $256 \times 256$ . In the long-range appearance loss function  $L_a$ , we estimate the depth of the images using DPT-DINOv2-base [37]. For pixel matching, we adopt Sinkhorn divergences [4] as an efficient approximation of the optimal transport algorithm and use a GPU implementation provided by GemoLoss [10] with the parameter  $\epsilon$  set to 0.01. In the high-level semantic loss function  $L_s$ , we extract image features using DINOv2-base [37] and compute the loss using features of the last hidden state.  $L_s$  is subjected to a warm-up period of 200 iterations. In Eq. 9, we set  $\lambda$  to 0.9. All experiments were conducted on RTX 3090 GPUs with the alignment process for each sample taking approximately 5 minutes and utilizing 4GB of memory.

<sup>3</sup><https://github.com/lkwq007/stablediffusion-infinity>

Table 1: Performance of different 3D generation models for compositional 3D assets generation.

Method	CLIP score $\uparrow$	PSNR $\uparrow$	SSIM $\uparrow$	LPIPS $\downarrow$
DreamGaussian [48]	0.807	13.280	0.802	0.240
Wonder3D [32]	0.801	13.689	0.807	0.238
LRM [14]	0.812	13.664	0.806	0.237
DreamGaussian-based REPARO (ours)	0.833	17.391	0.827	0.232
TripoSR-based REPARO (ours)	0.823	17.778	0.865	0.216

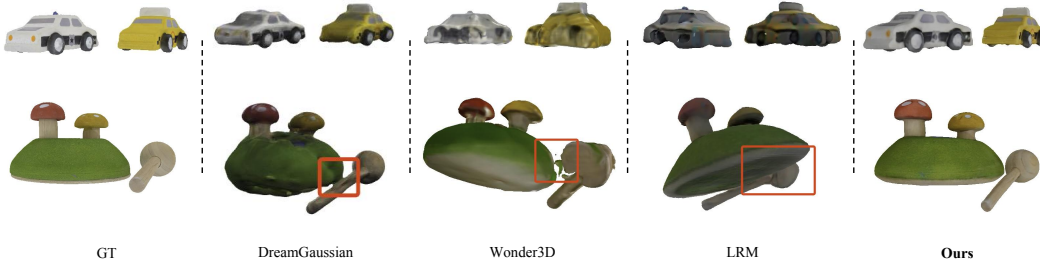


Figure 4: Qualitative comparison with different image-to-3D generation models.

To validate the effectiveness of our method, we selected 20 samples containing multiple objects from the Google Scanned Objects (GSO) dataset [8] as our test set. We used images from 18 views to compute quantitative metrics, including CLIP score [41], Peak signal-to-noise ratio (PSNR), the structural similarity (SSIM) [59], and Perceptual Similarity (LPIPS) [68]. Moreover, we also conducted a subjective evaluation of the generation quality for different models. We collected opinions from 40 participants. Participants selected the visually best subjective quality option among the generation results of 4 models for the same input image. We computed the preference score for each model by dividing the selection count of a specific model by the total selections, reflecting the human preference distribution for each model.

## 4.2 Main results

**Quantitative experiment.** Table 1 compares the performance (CLIP score, PSNR, SSIM, and LPIPS) of various methods for reconstructing 3D assets of multiple objects using one reference image. DreamGaussian-based REPARO and TripoSR-based REPARO, our proposed methods, show significant improvements over baseline methods (DreamGaussian [48], Wonder3D [32], and LRM [14]). DreamGaussian-based REPARO achieves 83.3% CLIP score, 17.391 PSNR, 0.827 SSIM, and 0.232 LPIPS, indicating better alignment between reconstructed 3D assets and ground-truth 3D assets. TripoSR-based REPARO exhibits superior performance in PSNR (17.778) and SSIM (0.865) and the lowest LPIPS (0.216), highlighting its exceptional quality in image reconstruction and perceptual similarity. These results show that better reconstruction quality on single objects is beneficial for structural similarity and perceptual similarity during differentiable rendering.

**Qualitative experiment.** Some qualitative comparison results are shown in Figure 4, where our TripoSR-based REPARO can produce high-quality 3D assets with multiple objects. By contrast, DreamGaussian [48], Wonder3D [32], and LRM [14] have problems in layout and completeness, since they possess preferences on an individual object.

**User study.** We conducted a user study to compare our method with others. We gathered 280 responses from 40 human participants. Each participant was shown a reference image alongside four 3D assets (including our model and baseline model DreamGaussian [48], Wonder3D [32] and LRM [14]) simultaneously and asked to select the most realistic assets based on geometry, texture quality, and accurate placement. All options were presented in a randomized order with no time constraints. Figure 5 illustrates that our approach significantly outperformed previous methods in terms of human preference.

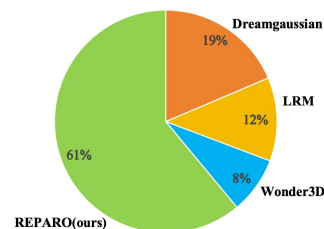


Figure 5: User study of different models.



### 4.3 Ablation study

Table 2: Comparison of different loss functions in differentiable rendering.

(a) DreamGaussian-based REPARO.						(b) TripoSR-based REPARO.					
$L_a$	$L_s$	CLIP score $\uparrow$	PSNR $\uparrow$	SSIM $\uparrow$	LPIPS $\downarrow$	$L_a$	$L_s$	CLIP score $\uparrow$	PSNR $\uparrow$	SSIM $\uparrow$	LPIPS $\downarrow$
$\checkmark$		0.833	17.296	0.826	0.233	$\checkmark$		0.822	17.765	0.865	0.216
	$\checkmark$	0.809	17.820	0.849	0.210		$\checkmark$	0.813	17.906	0.867	0.212
$\checkmark$	$\checkmark$	0.833	17.391	0.827	0.232	$\checkmark$	$\checkmark$	0.823	17.778	0.865	0.216

**Ablation for different loss functions in differentiable rendering.** We conducted ablation experiments on different loss components in Eq. 9, with the results presented in Table 2. The results indicate that incorporating the high-level semantic loss function  $L_s$  can bring improvements in both SSIM and perceptual LPIPS. However, the enhancement in CLIP score is not as pronounced. Additionally, when only  $L_s$  is used, there is a notable decrease in CLIP score. For instance, in the DreamGaussian-based model, the CLIP score decreased by 2.1%. This suggests that relying solely on feature supervision can reduce the effectiveness of layout alignment.

**Ablation for long-range appearance loss term.** As shown in Eq. 5, our proposed long-range appearance loss  $L_a$  incorporates RGB color distance, position distance, and depth value distance. More importantly, we use the optimal transport to compute pixel matching from a global perspective, thereby obtaining long-range correspondences. Quantitative results in Table 3 demonstrate that in the DreamGaussian-based model, introducing long-range correspondence results in a 2.8% improvement in CLIP score; in the TripoSR-based model, it results in a 4.5% improvement in CLIP score. However, after incorporating long-range correspondence, PSNR, SSIM, and LPIPS metrics are inferior compared to the local-range loss function. We conducted further qualitative studies (please see appendix) and found that without pixel matching, the layout cannot be aligned with the reference image. Additionally, when position distance and depth distance are introduced separately, there is no significant change in quantitative results, but there is a noticeable improvement in qualitative results, as illustrated in Figure 6.

Table 3: Comparison of different information used in appearance loss  $L_a$  (Eq. 5). OT represents whether to use the optimal transport algorithm to obtain pixel matching.

(a) DreamGaussian-based REPARO.						(b) TripoSR-based REPARO.					
Info in $L_a$	OT	CLIP $\uparrow$	PSNR $\uparrow$	SSIM $\uparrow$	LPIPS $\downarrow$	Info in $L_a$	OT	CLIP $\uparrow$	PSNR $\uparrow$	SSIM $\uparrow$	LPIPS $\downarrow$
RGB	$\times$	0.800	18.054	0.853	0.206	RGB	$\times$	0.774	17.918	0.868	0.216
RGB	$\checkmark$	0.828	17.009	0.821	0.245	RGB	$\checkmark$	0.819	17.837	0.865	0.215
RGBXY	$\checkmark$	0.828	17.069	0.821	0.243	RGBXY	$\checkmark$	0.823	17.847	0.865	0.213
RGBDXY	$\checkmark$	0.833	17.391	0.827	0.232	RGBDXY	$\checkmark$	0.822	17.765	0.865	0.216

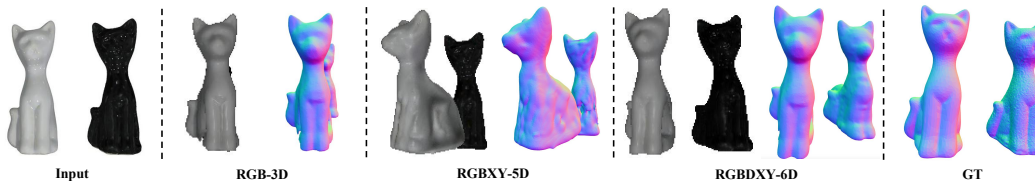


Figure 6: Qualitative comparison for different terms in the appearance loss  $L_a$  (Eq. 5).

## 5 Conclusion and Discussion

In conclusion, we introduce REPARO, a comprehensive approach for generating compositional 3D scenes from single images. Our REPARO addresses the multi-object issue by decomposing the scene into individual objects, reconstructing their 3D meshes, and optimizing their layout through differentiable rendering. During differentiable rendering, we incorporate an optimal transport-based

long-range appearance loss which considers RGBDX information, and a high-level semantic loss which aligns the feature correspondence. Consequently, REPARO is able to obtain multi-object 3D assets with visual-spatial arrangement and contextual consistency. Nevertheless, our findings indicate a discrepancy between the quantitative and qualitative results in the evaluation of multi-objective 3D assets. Specifically, the quantitative results show improvement but the qualitative results exhibit only marginal enhancement. Hence, it is imperative to develop evaluation methods for multi-object 3D assets in future research.

## References

- [1] Rui Chen, Yongwei Chen, Ningxin Jiao, and Kui Jia. Fantasia3d: Disentangling geometry and appearance for high-quality text-to-3d content creation. In *Proceedings of the IEEE/CVF International Conference on Computer Vision (ICCV)*, October 2023. 3
- [2] Yongwei Chen, Tengfei Wang, Tong Wu, Xingang Pan, Kui Jia, and Ziwei Liu. Comboverse: Compositional 3d assets creation using spatially-aware diffusion guidance. *arXiv preprint arXiv:2403.12409*, 2024. 4
- [3] Zilong Chen, Feng Wang, Yikai Wang, and Huaping Liu. Text-to-3d using gaussian splatting, 2024. 4
- [4] Marco Cuturi. Sinkhorn distances: Lightspeed computation of optimal transport. *Advances in neural information processing systems*, 26, 2013. 6, 7
- [5] Matt Deitke, Ruoshi Liu, Matthew Wallingford, Huong Ngo, Oscar Michel, Aditya Kusupati, Alan Fan, Christian Laforte, Vikram Voleti, Samir Yitzhak Gadre, Eli VanderBilt, Aniruddha Kembhavi, Carl Vondrick, Georgia Gkioxari, Kiana Ehsani, Ludwig Schmidt, and Ali Farhadi. Objaverse-xl: A universe of 10m+ 3d objects. *arXiv preprint arXiv:2307.05663*, 2023. 4
- [6] Matt Deitke, Dustin Schwenk, Jordi Salvador, Luca Weihs, Oscar Michel, Eli VanderBilt, Ludwig Schmidt, Kiana Ehsani, Aniruddha Kembhavi, and Ali Farhadi. Objaverse: A universe of annotated 3d objects, 2022. 4
- [7] Laura Downs, Anthony Francis, Nate Koenig, Brandon Kinman, Ryan Hickman, Krista Reymann, Thomas B McHugh, and Vincent Vanhoucke. Google scanned objects: A high-quality dataset of 3d scanned household items. In *2022 International Conference on Robotics and Automation (ICRA)*, pages 2553–2560. IEEE, 2022. 3
- [8] Laura Downs, Anthony Francis, Nate Koenig, Brandon Kinman, Ryan Hickman, Krista Reymann, Thomas B McHugh, and Vincent Vanhoucke. Google scanned objects: A high-quality dataset of 3d scanned household items. In *2022 International Conference on Robotics and Automation (ICRA)*, pages 2553–2560. IEEE, 2022. 8
- [9] Dave Epstein, Ben Poole, Ben Mildenhall, Alexei A Efros, and Aleksander Holynski. Disentangled 3d scene generation with layout learning. *arXiv preprint arXiv:2402.16936*, 2024. 4
- [10] Jean Feydy, Joan Glaunès, Benjamin Charlier, and Michael Bronstein. Fast geometric learning with symbolic matrices. *Advances in Neural Information Processing Systems*, 33, 2020. 7
- [11] Thomas Funkhouser, Michael Kazhdan, Philip Shilane, Patrick Min, William Kiefer, Ayellet Tal, Szymon Rusinkiewicz, and David Dobkin. Modeling by example. 23(3):652–663, 2004. 4
- [12] Gege Gao, Weiyang Liu, Anpei Chen, Andreas Geiger, and Bernhard Schölkopf. Graphdreamer: Compositional 3d scene synthesis from scene graphs. In *Conference on Computer Vision and Pattern Recognition (CVPR)*, 2024. 3, 4
- [13] Zheng Ge, Songtao Liu, Zeming Li, Osamu Yoshie, and Jian Sun. Ota: Optimal transport assignment for object detection. In *Proceedings of the IEEE/CVF conference on computer vision and pattern recognition*, pages 303–312, 2021. 6
- [14] Yicong Hong, Kai Zhang, Jiuxiang Gu, Sai Bi, Yang Zhou, Difan Liu, Feng Liu, Kalyan Sunkavalli, Trung Bui, and Hao Tan. Lrm: Large reconstruction model for single image to 3d. *arXiv preprint arXiv:2311.04400*, 2023. 4, 8
- [15] Ajay Jain, Ben Mildenhall, Jonathan T Barron, Pieter Abbeel, and Ben Poole. Zero-shot text-guided object generation with dream fields. In *Proceedings of the IEEE/CVF conference on computer vision and pattern recognition*, pages 867–876, 2022. 3

- [16] Bernhard Kerbl, Georgios Kopanas, Thomas Leimkühler, and George Drettakis. 3d gaussian splatting for real-time radiance field rendering. *ACM Transactions on Graphics*, 42(4), July 2023. 3, 4
- [17] Diederik P. Kingma and Jimmy Ba. Adam: A method for stochastic optimization. In *International Conference on Learning Representations, ICLR*, 2015. 6, 7
- [18] Alexander Kirillov, Eric Mintun, Nikhila Ravi, Hanzi Mao, Chloe Rolland, Laura Gustafson, Tete Xiao, Spencer Whitehead, Alexander C Berg, Wan-Yen Lo, et al. Segment anything. In *Proceedings of the IEEE/CVF International Conference on Computer Vision*, pages 4015–4026, 2023. 5, 7
- [19] Samuli Laine, Janne Hellsten, Tero Karras, Yeongho Seol, Jaakko Lehtinen, and Timo Aila. Modular primitives for high-performance differentiable rendering. *ACM Transactions on Graphics*, 39(6), 2020. 5, 7
- [20] Chenghao Li, Chaoning Zhang, Atish Waghvase, Lik-Hang Lee, Francois Rameau, Yang Yang, Sung-Ho Bae, and Choong Seon Hong. Generative ai meets 3d: A survey on text-to-3d in aigc era. *arXiv preprint arXiv:2305.06131*, 2023. 1
- [21] Ming Li, Pan Zhou, Jia-Wei Liu, Jussi Keppo, Min Lin, Shuicheng Yan, and Xiangyu Xu. Instant3d: Instant text-to-3d generation. *International Journal of Computer Vision*, pages 1–17, 2024. 3
- [22] Tzu-Mao Li, Miika Aittala, Frédo Durand, and Jaakko Lehtinen. Differentiable monte carlo ray tracing through edge sampling. *ACM Transactions on Graphics (TOG)*, 37(6):1–11, 2018. 5
- [23] Zhiqi Li, Yiming Chen, Lingzhe Zhao, and Peidong Liu. Controllable text-to-3d generation via surface-aligned gaussian splatting, 2024. 4
- [24] Jingbo Zhang<sup>3</sup> Zhihao Liang<sup>4</sup> Jing Liao, Yan-Pei Cao, and Ying Shan. Advances in 3d generation: A survey. *arXiv preprint arXiv:2401.17807*, 2024. 1
- [25] Chen-Hsuan Lin, Jun Gao, Luming Tang, Towaki Takikawa, Xiaohui Zeng, Xun Huang, Karsten Kreis, Sanja Fidler, Ming-Yu Liu, and Tsung-Yi Lin. Magic3d: High-resolution text-to-3d content creation. In *Proceedings of the IEEE/CVF Conference on Computer Vision and Pattern Recognition (CVPR)*, pages 300–309, June 2023. 1, 3
- [26] Yiqi Lin, Hao Wu, Ruichen Wang, Haonan Lu, Xiaodong Lin, Hui Xiong, and Lin Wang. Towards language-guided interactive 3d generation: Llms as layout interpreter with generative feedback. *arXiv preprint arXiv:2305.15808*, 2023. 4
- [27] Yukang Lin, Haonan Han, Chaoqun Gong, Zunnan Xu, Yachao Zhang, and Xiu Li. Consistent123: One image to highly consistent 3d asset using case-aware diffusion priors. *arXiv preprint arXiv:2309.17261*, 2023. 1, 4
- [28] Minghua Liu, Ruoxi Shi, Linghao Chen, Zhuoyang Zhang, Chao Xu, Xinyue Wei, Hansheng Chen, Chong Zeng, Jiayuan Gu, and Hao Su. One-2-3-45++: Fast single image to 3d objects with consistent multi-view generation and 3d diffusion. *arXiv preprint arXiv:2311.07885*, 2023. 4
- [29] Minghua Liu, Chao Xu, Haiyan Jin, Linghao Chen, Mukund Varma T, Zexiang Xu, and Hao Su. One-2-3-45: Any single image to 3d mesh in 45 seconds without per-shape optimization. *Advances in Neural Information Processing Systems*, 36, 2024. 4
- [30] Ruoshi Liu, Rundi Wu, Basile Van Hoorick, Pavel Tokmakov, Sergey Zakharov, and Carl Vondrick. Zero-1-to-3: Zero-shot one image to 3d object. In *Proceedings of the IEEE/CVF International Conference on Computer Vision*, pages 9298–9309, 2023. 1, 4
- [31] Yuan Liu, Cheng Lin, Zijiao Zeng, Xiaoxiao Long, Lingjie Liu, Taku Komura, and Wenping Wang. Syncdreamer: Generating multiview-consistent images from a single-view image. *arXiv preprint arXiv:2309.03453*, 2023. 4
- [32] Xiaoxiao Long, Yuan-Chen Guo, Cheng Lin, Yuan Liu, Zhiyang Dou, Lingjie Liu, Yuexin Ma, Song-Hai Zhang, Marc Habermann, Christian Theobalt, et al. Wonder3d: Single image to 3d using cross-domain diffusion. *arXiv preprint arXiv:2310.15008*, 2023. 4, 8
- [33] Luke Melas-Kyriazi, Christian Rupprecht, Iro Laina, and Andrea Vedaldi. Realfusion: 360 reconstruction of any object from a single image. In *2023 IEEE/CVF Conference on Computer Vision and Pattern Recognition (CVPR)*, 2023. 1, 4

- [34] Ben Mildenhall, Pratul P. Srinivasan, Matthew Tancik, Jonathan T. Barron, Ravi Ramamoorthi, and Ren Ng. Nerf: Representing scenes as neural radiance fields for view synthesis. In Andrea Vedaldi, Horst Bischof, Thomas Brox, and Jan-Michael Frahm, editors, *Proceedings of the European conference on computer vision (ECCV)*, pages 405–421, Cham, 2020. Springer International Publishing. 1, 3, 4
- [35] Nasir Mohammad Khalid, Tianhao Xie, Eugene Belilovsky, and Tiberiu Popa. Clip-mesh: Generating textured meshes from text using pretrained image-text models. In *SIGGRAPH Asia 2022 Conference Papers*, SA '22, 2022. 3
- [36] Nasir Mohammad Khalid, Tianhao Xie, Eugene Belilovsky, and Tiberiu Popa. Clip-mesh: Generating textured meshes from text using pretrained image-text models. In *SIGGRAPH Asia 2022 conference papers*, pages 1–8, 2022. 3
- [37] Maxime Oquab, Timothée Darcet, Théo Moutakanni, Huy Vo, Marc Szafraniec, Vasil Khalidov, Pierre Fernandez, Daniel Haziza, Francisco Massa, Alaaeldin El-Nouby, et al. Dinov2: Learning robust visual features without supervision. *arXiv preprint arXiv:2304.07193*, 2023. 7
- [38] Ryan Po and Gordon Wetzstein. Compositional 3d scene generation using locally conditioned diffusion. *arXiv preprint arXiv:2303.12218*, 2023. 4
- [39] Ben Poole, Ajay Jain, Jonathan T Barron, and Ben Mildenhall. Dreamfusion: Text-to-3d using 2d diffusion. *arXiv preprint arXiv:2209.14988*, 2022. 1, 3
- [40] Guocheng Qian, Jinjie Mai, Abdullah Hamdi, Jian Ren, Aliaksandr Siarohin, Bing Li, Hsin-Ying Lee, Ivan Skorokhodov, Peter Wonka, Sergey Tulyakov, and Bernard Ghanem. Magic123: One image to high-quality 3d object generation using both 2d and 3d diffusion priors. *arXiv preprint arXiv:2306.17843*, 2023. 4
- [41] Alec Radford, Jong Wook Kim, Chris Hallacy, Aditya Ramesh, Gabriel Goh, Sandhini Agarwal, Girish Sastry, Amanda Askell, Pamela Mishkin, Jack Clark, et al. Learning transferable visual models from natural language supervision. In *International conference on machine learning*, pages 8748–8763. PMLR, 2021. 3, 8
- [42] Amit Raj, Srinivas Kaza, Ben Poole, Michael Niemeyer, Nataniel Ruiz, Ben Mildenhall, Shiran Zada, Kfir Aberman, Michael Rubinstein, Jonathan Barron, et al. Dreambooth3d: Subject-driven text-to-3d generation. In *Proceedings of the IEEE/CVF International Conference on Computer Vision*, pages 2349–2359, 2023. 3
- [43] Junyoung Seo, Wooseok Jang, Min-Seop Kwak, Hyeonsu Kim, Jaehoon Ko, Junho Kim, Jin-Hwa Kim, Jiyoung Lee, and Seungryong Kim. Let 2d diffusion model know 3d-consistency for robust text-to-3d generation, 2024. 4
- [44] Ruoxi Shi, Hansheng Chen, Zhuoyang Zhang, Minghua Liu, Chao Xu, Xinyue Wei, Linghao Chen, Chong Zeng, and Hao Su. Zero123++: a single image to consistent multi-view diffusion base model. *arXiv preprint arXiv:2310.15110*, 2023. 4
- [45] Yichun Shi, Peng Wang, Jianglong Ye, Mai Long, Kejie Li, and Xiao Yang. Mvdream: Multi-view diffusion for 3d generation. *arXiv preprint arXiv:2308.16512*, 2023. 4
- [46] Yukai Shi, Jianan Wang, He Cao, Boshi Tang, Xianbiao Qi, Tianyu Yang, Yukun Huang, Shilong Liu, Lei Zhang, and Heung-Yeung Shum. Toss: High-quality text-guided novel view synthesis from a single image. *arXiv preprint arXiv:2310.10644*, 2023. 4
- [47] Ryo Suzuki, Adnan Karim, Tian Xia, Hooman Hedayati, and Nicolai Marquardt. Augmented reality and robotics: A survey and taxonomy for ar-enhanced human-robot interaction and robotic interfaces. In *Proceedings of the 2022 CHI Conference on Human Factors in Computing Systems*, pages 1–33, 2022. 1
- [48] Jiayang Tang, Jiawei Ren, Hang Zhou, Ziwei Liu, and Gang Zeng. Dreamgaussian: Generative gaussian splatting for efficient 3d content creation. *arXiv preprint arXiv:2309.16653*, 2023. 4, 5, 7, 8
- [49] Junshu Tang, Tengfei Wang, Bo Zhang, Ting Zhang, Ran Yi, Lizhuang Ma, and Dong Chen. Make-it-3d: High-fidelity 3d creation from a single image with diffusion prior. In *Proceedings of the IEEE/CVF International Conference on Computer Vision (ICCV)*, pages 22819–22829, October 2023. 1, 4
- [50] Konstantinos Tertikas, Despoina Paschalidou, Boxiao Pan, Jeong Joon Park, Mikaela Angelina Uy, Ioannis Emiris, Yannis Avrithis, and Leonidas Guibas. Generating part-aware editable 3d shapes without 3d supervision. In *Proceedings of the IEEE/CVF Conference on Computer Vision and Pattern Recognition*, pages 4466–4478, 2023. 4

- [51] Dmitry Tochilkin, David Pankratz, Zexiang Liu, Zixuan Huang, , Adam Letts, Yangguang Li, Ding Liang, Christian Laforte, Varun Jampani, and Yan-Pei Cao. Triposr: Fast 3d object reconstruction from a single image. *arXiv preprint arXiv:2403.02151*, 2024. 4, 7
- [52] Alex Trevithick and Bo Yang. Grf: Learning a general radiance field for 3d representation and rendering. In *Proceedings of the IEEE/CVF International Conference on Computer Vision*, pages 15182–15192, 2021. 3
- [53] Ashish Vaswani, Noam Shazeer, Niki Parmar, Jakob Uszkoreit, Llion Jones, Aidan N Gomez, Lukasz Kaiser, and Illia Polosukhin. Attention is all you need. *Advances in neural information processing systems*, 30:5998–6008, 2017. 4
- [54] Alexander Vilesov, Pradyumna Chari, and Achuta Kadambi. Cg3d: Compositional generation for text-to-3d via gaussian splatting. *arXiv preprint arXiv:2311.17907*, 2023. 4
- [55] Can Wang, Menglei Chai, Mingming He, Dongdong Chen, and Jing Liao. Clip-nerf: Text-and-image driven manipulation of neural radiance fields. In *2022 IEEE/CVF Conference on Computer Vision and Pattern Recognition (CVPR)*, pages 3825–3834, 2022. 3
- [56] Haochen Wang, Xiaodan Du, Jiahao Li, Raymond A. Yeh, and Greg Shakhnarovich. Score jacobian chaining: Lifting pretrained 2d diffusion models for 3d generation, 2022. 4
- [57] Zhaoning Wang, Ming Li, and Chen Chen. Luciddreaming: Controllable object-centric 3d generation. *arXiv preprint arXiv:2312.00588*, 2023. 4
- [58] Zhengyi Wang, Cheng Lu, Yikai Wang, Fan Bao, Chongxuan Li, Hang Su, and Jun Zhu. Prolificdreamer: High-fidelity and diverse text-to-3d generation with variational score distillation. *Advances in Neural Information Processing Systems*, 36, 2024. 1, 3
- [59] Zhou Wang, Alan C Bovik, Hamid R Sheikh, and Eero P Simoncelli. Image quality assessment: from error visibility to structural similarity. *IEEE transactions on image processing*, 13(4):600–612, 2004. 8
- [60] Haohan Weng, Tianyu Yang, Jianan Wang, Yu Li, Tong Zhang, CL Chen, and Lei Zhang. Consistent123: Improve consistency for one image to 3d object synthesis. *arXiv preprint arXiv:2310.08092*, 2023. 4
- [61] Jiankai Xing, Fujun Luan, Ling-Qi Yan, Xuejun Hu, Houde Qian, and Kun Xu. Differentiable rendering using rgbxy derivatives and optimal transport. *ACM Transactions on Graphics (TOG)*, 41(6):1–13, 2022. 5, 6, 7
- [62] Jiale Xu, Xintao Wang, Weihao Cheng, Yan-Pei Cao, Ying Shan, Xiaohu Qie, and Shenghua Gao. Dream3d: Zero-shot text-to-3d synthesis using 3d shape prior and text-to-image diffusion models. In *Proceedings of the IEEE/CVF Conference on Computer Vision and Pattern Recognition (CVPR)*, pages 20908–20918, June 2023. 3
- [63] Yinghao Xu, Hao Tan, Fujun Luan, Sai Bi, Peng Wang, Jiahao Li, Zifan Shi, Kalyan Sunkavalli, Gordon Wetzstein, Zexiang Xu, and Kai Zhang. Dmv3d: Denoising multi-view diffusion using 3d large reconstruction model, 2023. 4
- [64] Han Yan, Yang Li, Zhennan Wu, Shenzhou Chen, Weixuan Sun, Taizhang Shang, Weizhe Liu, Tian Chen, Xiangqiang Dai, Chao Ma, et al. Frankenstein: Generating semantic-compositional 3d scenes in one tri-plane. *arXiv preprint arXiv:2403.16210*, 2024. 4
- [65] Taoran Yi, Jiemin Fang, Junjie Wang, Guanjun Wu, Lingxi Xie, Xiaopeng Zhang, Wenyu Liu, Qi Tian, and Xinggang Wang. Gaussiandreamer: Fast generation from text to 3d gaussians by bridging 2d and 3d diffusion models. In *CVPR*, 2024. 4
- [66] Xuening Yuan, Hongyu Yang, Yueming Zhao, and Di Huang. Dreamscape: 3d scene creation via gaussian splatting joint correlation modeling. *arXiv preprint arXiv:2404.09227*, 2024. 4
- [67] Junwu Zhang, Zhenyu Tang, Yatian Pang, Xinhua Cheng, Peng Jin, Yida Wei, Wangbo Yu, Munan Ning, and Li Yuan. Repaint123: Fast and high-quality one image to 3d generation with progressive controllable 2d repainting. *arXiv preprint arXiv:2312.13271*, 2023. 4
- [68] Richard Zhang, Phillip Isola, Alexei A Efros, Eli Shechtman, and Oliver Wang. The unreasonable effectiveness of deep features as a perceptual metric. In *Proceedings of the IEEE conference on computer vision and pattern recognition*, pages 586–595, 2018. 8

## A Appendix

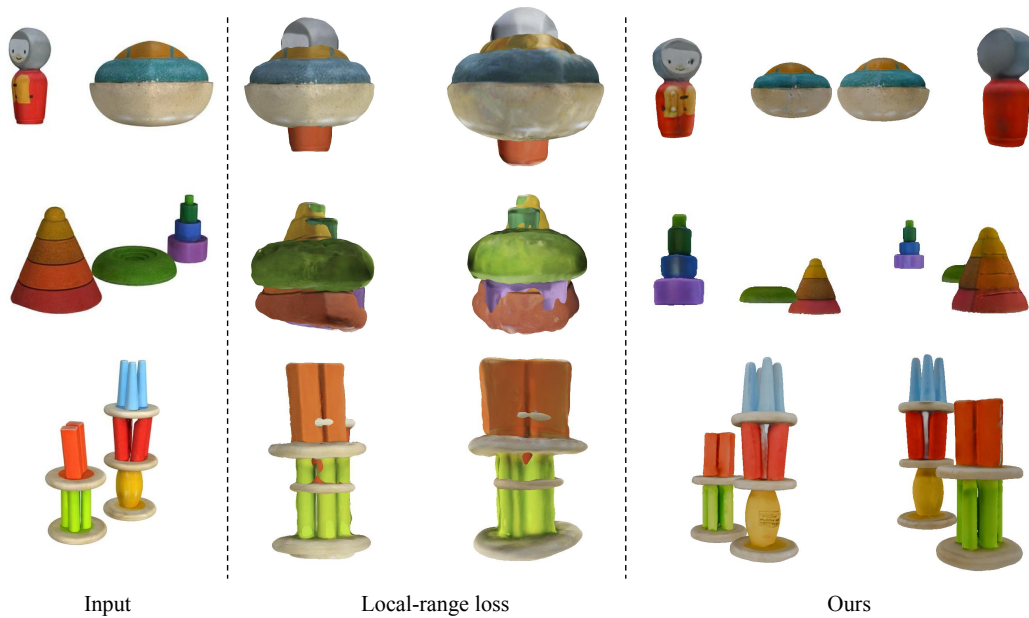


Figure 7: Qualitative comparison for local-range loss and our loss.

In Table 3, the loss term using only RGB color information without pixel matching obtains better PSNR, SSIM, and LPIPS performance compared to the method with long-range pixel matching. We show some qualitative results in Figure 7. These results demonstrate that the layout is not aligned with the reference image when using the local range loss term. By contrast, the proposed long-range loss term can optimize the scene parameters and align the layout with the reference image.